www.sciencemag.org/cgi/content/full/343/6173/857/DC1

Supplementary Materials for

Dendritic Inhibition in the Hippocampus Supports Fear Learning

Matthew Lovett-Barron, Patrick Kaifosh, Mazen A. Kheirbek, Nathan Danielson, Jeffrey D. Zaremba, Thomas R. Reardon, Gergely F. Turi, René Hen, Boris V. Zemelman, Attila Losonczy*

*Corresponding author. E-mail: al2856@columbia.edu

Published 21 February 2014, *Science* **343**, 857 (2014)
DOI: 10.1126/science.1247485

This PDF file includes:

Materials and Methods

All experiments were conducted in accordance with the US National Institutes of Health guidelines and with the approval of the Columbia University and New York State Psychiatry Institute Institutional Animal Care and Use Committees.

Mice and Viruses

In all experiments we used adult mice of either sex, that were either wild-type C57/Bl6 mice, ChAT-cre mice (Jackson, #006410), or the hemizygous offspring of Som-Cre or Pvalb-cre mice with the Ai9 reporter line (loxP-STOP-loxP-tdTomato Cre reporter strain B6;129S6-Gt(ROSA)26Sortm9(CAG-tdTomato)Hze/J (Jackson Laboratory)) on a C57/Bl6 background, have previously reported (*25*).

We used the following viruses: rAAV2/1(*synapsin-PSAM*$^{L\text{-}141F}$*-GlyR*), rAAV2/7(*Synapsin-PSAM*$^{L\text{-}141F}$*-GlyR*)^{cre} (*25,30*), rAAV2/1(*Synapsin-GCaMP5G*) (*29,34*), rAAV2/7(*Synapsin-GCaMP5G*)^{cre}, rAAV2/1(*Synapsin-GCaMP6f*), rAAV2/7(*Synapsin-GCaMP6f*)^{cre} (*52*; Penn vector core), rAAV2/7(*Synapsin-eNpHR3.0-eGFP*)^{cre}, rAAV2/7(*Synapsin-tdTomato*)^{cre}, or rAAV2/7(*Synapsin-eGFP*)^{cre}. For targeting ChAT+ neurons in the medial septum, rAAV2/1(*ef1α-DIO-GCaMP6f*)^{cre} was created by cloning the GCaMP6f gene (Addgene 40755) into the Cre-conditional vector, rAAV-*ef1α*-DIO-hChR2(H134R)-EYFP-WPRE-pA (Addgene 20298), replacing the existing hChR2-EYFP insert. Restriction sites 5' NheI and 3' AscI were used, and only the core of GCaMP6f was maintained after removing the 5' 6xHis tag. A chimeric serotype 1+2 of AAV was prepared (*64*) for stereotaxic injection. This specific serotype and viral promoter were required to gain reliable expression in ChAT-positive cells, as *synapsin* (serotypes 2/1 & 2/7) and *CAG* (serotype 5) viruses were ineffective for labeling these neurons. Stereotaxic viral injections were performed using a Nanoject syringe, as described previously *(25,29).* Recordings from eNpHR3.0-GFP/Som+ interneurons in CA1 were performed as described previously (*25*), and cells were stimulated using the same 593nm laser used for *in vivo* experiments.

Surgery

Hippocampal window

Hippocampal window implant surgeries were performed as described previously (*29,35*). Briefly, we anesthetized mice with isoflurane and treated them with buprenorphine (0.1 mg/kg, subcutaneous) to minimize post-operative discomfort. We exposed the skull and drilled a 3-mm diameter circle centered over left dorsal CA1, matching the size of the cannula window to be implanted. We removed the bone and dura, and then slowly aspirated cortex covering the hippocampus while constantly irrigating with chilled cortex buffer until the external capsule was exposed. If the alveus (anterior-posterior fibers) became exposed, surgery was terminated. Otherwise, we implanted the sterilized window implant by wedging it into place, and secured the top of the cannula to the skull and stainless steel headpost with grip cement, leaving it to dry for 15–20 min before returning mice to the home cage (awake and mobile in 5–20 min). We monitored mice every 12 hours for three days after surgery, administering buprenorphine to minimize any signs of discomfort.

Optical fibers

We used published techniques for the construction of chronically dwelling optical fibers and patch cables for optogenetic behavioral procedures (*65*). For all experiments, a 200 μm core, 0.37 numerical aperture (NA) multimode fiber was used for optical stimulation via a patch cable connected to either a 100 mw 593.5 or 473 nm laser diode. Adult mice were surgically implanted with fiber optic cannulas using published protocols (*65*).

Head-fixed stimulus presentation and behavioral readout

We developed a flexible system for combining two-photon imaging with microcontroller-driven stimulus presentation and behavioral read-out, as previously described (*29*). Briefly, tones were presented with speakers near each of the mouse's ears, light flashes lasting 200 ms were delivered with a red LED, and odor stimuli and air-puffs were delivered via separate solenoid valves to gate airflow from a compressed air tank to a tube ending in a pipette tip facing the mouse's snout. Odor was delivered with lower pressure air, and passed through a filter covered in a 50:50 mixture of odorant with mineral oil (50 μL). We tracked locomotion by measuring treadmill wheel rotation,

recorded as changes in voltage across an infrared photo-transistor as wheel spokes blocked light from an infrared LED. Electrical signals encoding mouse behavior and stimulus presentation were collected with an analog to digital converter, which was synchronized with two-photon imaging by a common trigger pulse.

We used headpost-implanted adult mice for all experiments. In the case of hf-CFC experiment, starting 3–7 days after implantation we water-restricted mice (>85% pre-deprivation weight) and habituated them to handling and head-fixation. Within 3 or 4 sessions, mice could undergo extended head-fixation while appearing calm, but alert, and periodically running while freely licking for small-volume (~0.5 μl/lick) water rewards during imaging sessions. During the hf-CFC task, mice could lick for water for 4.5 min – 1 m pre context, 3 min context, and 30 s post-context. This protocol was repeated twice a day for three days (Habituation, Conditioning, and Recall), with 1-3 hours between each context. Each context CS consisted of a distinct set of auditory, visual, olfactory, and tactile cues that we presented to mice using a microcontroller-driven stimulus presentation and behavioral recording system (**Fig. S1a**)(*29*). On the second day (Conditioning) we presented mice with both contexts again, but paired one context (CtxC) with a US: six air-puffs to the snout (200 ms, 0.1 Hz) during the final minute of the context. The other context was neutral and not paired with a US (CtxN). On the third day (Recall), we exposed mice to the conditioned context (CtxC) and the neutral context (CtxN) again, and assessed the rate of licking in each context.

For discrete stimulus presentation, we habituated mice to handling and head-fixation, but did not water-restrict them. We used a variable inter-stimulus interval of 20–40 s between stimuli, which were repeated 5–10 times for each modality in a pseudorandom order. To characterize responses to air-puffs of varying durations, we repeated stimulation with durations from 10 ms to 500 ms; each level was presented 3 times, interspersed with 200 ms tones.

Freely-moving behavior

Fear Conditioning – PSAM^{L141F}-GlyR experiments

Fear conditioning took place in fear-conditioning boxes that contained one clear plexiglass wall, three aluminum walls, and a stainless steel grid as a floor. All mice were

injected with PSEM^{89} (60 mg/kg i.p. in saline) 15 min prior to conditioning. The training session began with the onset of the houselight and fan, and anise scent was placed under the grid floor. In this one-trial contextual fear conditioning protocol, 180 s after placement of the mouse in the training context and onset of houselight and fan, mice received a single 2 s footshock of 1 mA. All freezing was measured before the single footshock. The mouse was taken out 15 s after termination of the footshock and returned to its home cage. The grid and the waste tray were cleaned with Sanicloths between runs. The recall session occurred 24 hours later in the same chamber, but without PSEM^{89} injection or footshocks. Mice were recorded by video cameras mounted above the conditioning chamber and were scored for freezing by an investigator blind to the experimental condition of the animal.

Fear Conditioning – Tone conditioning

All mice were injected with PSEM^{89} (60 mg/kg i.p. in saline) 15 min prior to conditioning. For cued fear conditioning, mice were trained in the same context as in CFC, except that a 20 s, 80 dB, 2 kHz pure tone was provided as the discrete cue CS, and a 2 s footshock that co-terminated with the tone was provided. This was repeated three times. Twenty-four hours later, mice were tested for cued fear in a novel context, in which the conditioning chamber was altered, the stainless steel grid floor was covered with a plastic panel and novel cage bedding, the chamber walls were covered and made circular using colored plastic inserts, the house fan and lights were turned off, and no scent was used. The tone was presented three times, and an investigator blind to condition scored freezing before the first tone presentation and during each tone presentation as a measure of cued fear.

Fear Conditioning – optogenetic experiments

In the case of optogenetic manipulations during conditioning, mice were quickly attached to the fiber optic patch cables (bilaterally) via a zirconia sleeve, then placed in a novel cage bottom for five minutes prior to being placed in the testing apparatus. The patch cables were interfaced to an FC/PC rotary joint, which was attached on the other end to a 593 nm laser diode that was controlled by a Master-8 stimulator, as previously described (*65*). In these experiments, mice were exposed to two 2 s shocks (1 mA) separated by one minute; shocks were paired with 6 s optogenetic stimulation (593 nm)

centered over the shock (Light-US condition) or shifted 30 s before each shock (Light-shift condition). All mice were processed for histology, and subjects were excluded from the study if the implant entered the hippocampus, if viral infection was not complete, or if the viral infection was not limited to CA1 Som+ interneurons.

Delayed non-match to sample

Mice were food-restricted for 1 day prior to experiments. Mice pursued sweetened condensed milk rewards (50% dilution, 30 µL) (*66*). Mice were injected with 60 mg/kg PSEM^{89} i.p., and tested in a delayed non-match to sample task in a y-maze from 10-35 min post-injection. Mice performed 10 trials, in which the mouse began in the start box, and consisting of a sample phase (shuffling of location across trials), a 30 s delay phase in the start box, and a sample phase, where the correct response is to go to the arm not yet visited. Between trials mice were moved to a clean cage for 60 s, and the location of the sample arm was shuffled. Animals were scored as the % correct trials, and trials were omitted if mice took >90 s on the sample phase, or >120 s on the choice phase.

2-photon imaging

We use an *in vivo* X-Y galvanometer-mounted mirror-based multi-photon microscopy system and an ultra-fast pulsed laser beam (920-nm wavelength; 20–40 mW average power at the back focal plane of the objective) controlled with an electro-optical modulator to excite GCaMP and tdTomato through a 40X objective. Distilled water or warmed cortex buffer (in the case of acute pharmacology experiments) served to connect the water immersion objective with the cannula. Green and red fluorescence were separated with an emission filter cube set (green, HQ525/70m-2p; red, HQ607/45m-2p; 575dcxr). Fluorescent light was detected with photomultiplier tubes (green GCaMP fluorescence, GaAsP PMT; red tdTomato fluorescence, multi-alkali PMT) operated with PrairieView software. Once mice were head-fixed, we used goniometers (Edmund Optics) to adjust the angle of the mouse's head up to 10 degrees to make the imaging window parallel to the objective. Time series were collected in red (tdTomato signal) and green (GCaMP signal) channels at 256 × 128 pixels covering 150 × 150 µm at 7.63 Hz (cell bodies, interneuron axons), or 256 × 256 pixels covering 75 × 75 µm at 4.02 Hz (CA3, LEC, and ChAT+ axons). Time-series were motion-corrected as

described in ref. *29*, adapted from methods established in ref. *36*. Regions of interest (ROIs) were manually drawn over corrected time-series in Image J (NIH), to isolate the somas or axons of cells of interest. Trials with running were excluded from summary analyses of sensory responses in interneurons and excitatory axons.

Local pharmacology during 2-photon imaging

For local pharmacology experiments, we replaced the glass coverslip with a plastic coverslip with a punctured hole (~200 μm diameter) (*29*). This hole was plugged by a plastic bar and Kwik-Sil. Instead of waiting several days to perform experiments, mice were habituated and tested 1–5 days after implants. Before imaging, we removed the plastic plug and filled the cannula with warmed (~32 °C) cortex buffer (125 mM NaCl, 5 mM KCl, 10 mM glucose, 10 mM HEPES, 2 mM $CaCl_2$ and 2 mM $MgCl_2$). After control imaging, we filled the cannula and fluid well for the objective with cortex buffer containing dissolved scopolamine (1 mM), pirenzepine (0.01-1 mM), mecamylamine (1 mM), NBQX (20 μM), PSEM^{89} (500 μM), or bicuculine (20 μM) and allowed 30-90 min for drug diffusion before imaging.

Identification of significantly responding PCs

Approximately 150-200 ROIs were drawn over putative PCs for each field of view. Statistically significant calcium transients were identified automatically using an approach similar to that described by ref. *36*. Briefly, negative deflections in the $\Delta F/F$ trace are assumed to be due to motion out of the z-plane. Because cells should move into the imaging plane with the same frequency they leave this plane, positive and negative deflections in the $\Delta F/F$ curve that are attributable to motion should occur at the same frequency. Therefore we calculate a false positive event detection rate by dividing the number of negative deflections for a given amplitude and duration by the number of positive deflections at the same magnitude and duration. As signal-to-noise ratio can vary on a per-cell basis, event amplitudes are calculated in terms of the standard-deviation (σ) of the $\Delta F/F$ trace, which provides an estimate of noise for the cell. Transient onsets are defined as the times when the $\Delta F/F$ exceeds 2 σ, and offset is defined as the time at which $\Delta F/F$ falls below 0.5 σ. A decaying exponential was fit by

least-squares to the false positive rate values, allowing for the determination of a minimum transient duration at each σ level at different confidence levels (**Fig. S12**).

We analyzed sensory responses in PCs using peri-stimulus-time-histograms (PSTHs). To calculate PSTHs, a binary activity function of time was computed for each cell, indicating whether it was in a significant calcium transient (95% confidence). Time series were aligned by stimulus time, and the binary-activity functions across stimulus presentations were averaged at each time point in a window +/- 20 frames from the stimulus, yielding a PSTH of the binary activity function for each cell and stimulus. The response-value was defined as the mean of the 20 post frames minus the mean of the 20 pre frames. To assess confidence, alignment times were shuffled 10000 times, yielding a distribution of response-values. A cell was deemed significantly responsive if the true response-value exceeded the 95th percentile of the shuffle distribution. For significantly-responsive cells, PSTHs of the ΔF/F traces were computed similarly. For the analysis of PSEM and bicuculine effects on PC population (**Fig. 5** and **Fig. S13**), fields of view containing fewer than 3% responsive cells were omitted.

Immunohistochemistry & confocal imaging

After imaging experiments, virally-injected mice were deeply anesthetized with isoflurane and perfused with 4% paraformaldehyde dissolved in 0.1 M phosphate-buffered saline (pH = 7.4). Brains were removed, sectioned at 50-60 µm and either mounted for confocal microscopy or processed for immunofluorescence staining. In mice expressing PSAM^{L141F}-GlyR, we performed immunostaining of the hybrid PSAM^{L141F}-GlyR channel as detailed previously (*25,29,30*), using Alexa 647–conjugated α-bungarotoxin (α-BTX, 1:3000), selective for the mutated α7-nAChR receptor binding site of PSAM^{L141F}-GlyR. Confocal stack images (40–50 slices, 1-2 µm optical thickness) were collected from dorsal CA1 region with a 20X objective. Stacks were collapsed into one z-plane, and cell bodies that were labeled for tdTomato and/or α-BTX Alexa 647 were counted in the *oriens/alveus* and/or *pyramidale* layers of CA1 (ImageJ, US National Institutes of Health), allowing for quantification of the density and overlap of neuronal expression. In mice expressing GCaMP6f in ChAT+ cells of the medial septum, slices were immunostained with ChAT antibodies (AB144P; Millipore; 1:500

dilution) and detected with 1:500 concentration of anti-goat DyLight 649 (Jackson ImmunoResearch). Confocal tile-stack images (2,535 slices, 1 μm optical thickness) from the medial septum were acquired using a (20X objective), and counted for GCaMP6f and ChAT co-localization as described above.

Data analysis

hf-CFC was scored by automated measurement of the rate of licks in each context (capacitive transients measured from metal water port), as described previously (*29*). Freely-moving conditioning was assessed by freezing scored by a trained observer blind to the experimental condition. Head-fixed contextual fear conditioning behavioral data, delayed non-match to sample behavioral data, and responses by stimulus and cell type were analyzed with two-way ANOVA, with repeated measures in cases that the same subject was used across multiple conditions. Pair-wise comparisons were performed with sign tests for paired data and Mann-Whitney U tests for unpaired data. Sign tests were used to assess pharmacological effects on calcium responses, and Mann-Whitney U tests were used to assess pharmacogenetic effects on head-fixed contextual fear conditioning and differences in running-related activity across cell types. PC population imaging data was analyzed with paired or unpaired t-tests in the cases of % active cells and transient durations, respectively. Statistical tests on imaging data were performed treating each field-of-view as an independent observation by averaging the responses from all simultaneously imaged ROIs. Statistical comparisons were 1-way or 2-way ANOVAs, with pairwise sign tests or unpaired Mann-Whitney U tests, or paired and unpaired t-tests. All tests were two-sided, and the type of statistical test is noted in each case. All summary data are presented as mean ± s.e.m. *p <0.05, **p <0.01, ***p <0.001.

Supplementary References

64) McClure, C., Cole, K.L., Wulff, P., Klugmann, M., and Murray, A.J. (2011). Production and titering of recombinant adeno-associated viral vectors. *J Vis Exp*, **57**, e3348, doi:10.3791/3348.

65) Kheirbek, M.A., *et al.* (2013). Differential control of learning and anxiety along the dorsoventral axis of the dentate gyrus. *Neuron,* **77**, 955-968.

66) Deacon, R.M.J., and Rawlins, J.N.P. (2006). T-maze alternation in the rodent. *Nature Protocols*, **1**, 7-12.

Supplementary Figures

Fig. S1. Details of hf-CFC task and controls

a) Details about the two contexts used in the hf-CFC task. **b**)-**e**) Control experiments for the hf-CFC task – of mice that received no experimental manipulation, some received surgical or behavioral treatments whereas others did not. None of these treatments altered hf-CFC performance. **b**) Implant and imaging control: 'Imaging' group (n = 9) – mice express GCaMP, have a hippocampal window implanted, and have CA1 imaged with a 2-photon microscope during hf-CFC. 'No imaging' group (n = 12) – mice are implanted with a headpost alone with no window surgery or imaging. Unpaired t-test: p = 0.705. **c**) Viral expression control: 'Virus' group (n = 11) – mice have received stereotaxic injections of a virus to express tdTomato, GFP, or GCaMP. 'No virus' group (n = 10) – mice received no viral injection. Unpaired t-test: p = 0.828. **d**) PSEM injection control: 'PSEM' group (n=11) – mice were injected with 60 mg/kg PSEM^{89} in saline i.p 15 min before conditioning in CtxC session. These mice were used as the control group in Figure 1e. 'No PSEM' group (n=10) – mice received no PSEM^{89} injection. Unpaired t-test: p = 0.252. **e**) Context identity control: 'CtxC = 1' group (n = 10) – mice were conditioned to Context 1 (CtxC), and Context 2 was neutral (CtxN). 'CtxC = 2' group (n = 11) – mice were conditioned to Context 2 (CtxC), and Context 1 was neutral (CtxN). Unpaired t-test: p = 0.652. f) Mean lick rates for each group in Fig.1e, displaying the mean total lick rate across all sessions (baseline for learning index), and the mean lick rate in recall of CtxC and CtxN.

Fig. S2. Viral expression of PSAM^{L141F}-GlyR in CA1 Som+ or Pvalb+ interneurons of dorsal CA1

a) Septo-temporal extent of viral expression of the ligand-gated Cl- channel PSAM^{L141F}-GlyR in dorsal CA1, revealed by α-bungarotoxin/Alexa647 (*α-BTX IHC*) immunostaining (example *Som-cre* and *Pvalb-cre* mice). **b**) Mean % of cre/tdTomato+ cells in CA1 that are also PSAM^{L141F}-GlyR+ in *Som-cre/Ai9* (5 sections) and in *Pvalb-cre/Ai9* (6 sections) mice. **c**) Counts in *Som-cre/Ai9* mice from panel b) were restricted to *oriens*, because a sparse subset of CA1 PCs in *pyramidale* express tdTomato developmentally, but do not express cre in adulthood.

Fig. S3. PSAM^{L141F}-GlyR inactivation of CA1 interneurons during freely-moving CFC and tone conditioning

a) Schematic of experimental protocol. Mice were injected with 30 mg/kg PSEM^{89} i.p. 15 min before CFC with a single 2 s/1 mA footshock, and are tested in a recall session 24 hours later without PSEM^{89}. **b**) Summary data for contextual freezing 24 hours later with *Som-cre* mice and *Pvalb-cre* mice, expressing either tdTomato or PSAM^{L141F}-GlyR in cre+ CA1 interneurons (2-way ANOVA, genotype x virus: $F_{(1,31)} = 5.43$, $p < 0.05$). *Som-cre* mice, control vs. PSAM^{L141F}-GlyR ($p < 0.05$); *Pvalb-cre* mice, control vs. PSAM^{L141F}-GlyR ($p = 0.75$), unpaired 2-tailed t-test. **c**) Summary data for tone-conditioning experiments with *Som-cre* and *Pvalb-cre* mice. Mice were injected with 60 mg/kg PSEM^{89} i.p. 15 min before conditioning with four 20 s tones terminating with a 2 s/1 mA footshock. Freezing was assessed 24 hours later in an altered context without PSEM^{89}, tested with four repetitions of 20 s tones. *Som-cre*: control, n=2; PSAM^{L141F}-

GlyR, n=2; p = 0.56, unpaired 2-tailed t-test. *Pvalb-cre*: control, n=4; PSAM^{L141F}-GlyR, n=4; p = 0.839, unpaired 2-tailed t-test.

Fig. S4. Effects of inactivating CA1 Som+ interneurons on learning is not a consequence of brain-state effects
Som-cre mice were injected with 60 mg/kg PSEM^{89} in saline i.p. 15 min before CtxC conditioning session, and CtxC recall session. Unpaired 2-tailed t-test: $p < 0.01$. Because these mice were similar to *Som-cre* mice injected with PSEM^{89} during conditioning alone, the two groups were merged for Fig. 1e.

Fig. S5. Inactivating CA1 Pvalb+ interneurons with PSAM^{L141F}-GlyR disrupts spatial working memory
a) Schematic of experimental protocol. Mice pursued sweetened condensed milk rewards (50% dilution, 30 µL). Mice were injected with 60 mg/kg PSEM^{89} i.p., and tested in a delayed non-match to sample task in a y-maze from 10-35 min post-injection. Mice went through 10 trials beginning in the start box, consisting of a sample phase (shuffling of location across trials), a 30 s delay phase in the start box, and a choice phase. The correct response in the choice phase is to collect a reward in the arm not yet visted, reflecting working memory in a natural foraging behavior. Between trials mice were moved to a clean cage for 60 s. **b**) Summary data for DNMS task, in *Som-cre* and *Pvalb-cre* mice (2-way ANOVA, genotype x virus: $F_{(1,23)} = 2.0$, $p = 0.172$). There was a significant main effect of virus ($p < 0.005$). *Som-cre* mice, Control vs. PSAM^{L141F}-GlyR ($p = 0.173$); *Pvalb-cre* mice, control vs. PSAM^{L141F}-GlyR ($p < 0.05$), Mann-Whitney U tests.

Fig. S6. Fraction of sensory-evoked responses by cell types in CA1
a) Expression of GCaMP5G in CA1 *oriens* interneurons of a *Som-cre/Ai9* mouse, including parallel recording from Som/tdTom+ and Som/tdTom- interneurons. **b**) Left: traces from example cells in panel *a* during the pseudorandom presentation of discrete sensory stimuli. Traces are concatenated together from 30 individual trials of air-puffs, tones, and lights. Middle: example averaged air-puff responses on an expanded time scale. Right: The same data represented as heat maps, with trials grouped by stimulus type. **c**) Summary data for GCaMP5G responses to discrete sensory stimuli in Som+ and Som- interneurons (*Som-cre/Ai9* mice), Pvalb+ interneurons (*Pvalb-cre/Ai9*), and pyramidal cells (both lines). $\Delta F/F$ is calculated using the difference between the 5 s before and after stimulus onset.

Fig. S7. Local pharmacological manipulation of imaged tissue
a) Spread of 1% Evans Blue (in cortex buffer) through the perforated imaging window over the timescale of pharmacological manipulation, followed by perfusion, fixation, and mounting. **b**) Concentration-dependence of m1AChR blockade on air-puff-evoked activity in Som+ interneurons. Each line is one Som+ cell (n=13 cells). **c**) Responses of pyramidal cells to air-puffs (see Supplementary Figure 12 & 13) are not significantly altered by the concentration of pirenzepine (100µM) required to block Som+ interneuron responses to air-puffs. We measured this as the duration of air-puff-evoked transients in

PCs active in both drug conditions (ctrl: 2.51 ± 0.3s, Pir.: 2.84 ± 0.5s, n = 5 cells; paired t-test), as in Fig. 5 and Fig. S13.

Fig. S8. Expression of GCaMP6f in ChAT+ neurons of the medial septum and imaging their axons in CA1

a) Top: Confocal images of the medial septum showing co-localization of virally expressed GCaMP6f and endogenous ChAT with ChAT immunohistochemistry. Bottom: Summary graph of co-localization of ChAT immunohistochemistry and GCaMP labeling (n = 3 section in 3 mice) in ChAT-cre mice injected with rAAV2/1(*ef1α-DIO-GCaMP6f*)^{cre} into the medial septum. **b**) More examples of FOVs from *oriens/alveus* in CA1 of ChAT+ mice, and the ROIs drawn to analyze axonal signals. **c**) Responsiveness of ChAT+ axons to locomotion on the treadmill.

Fig. S9. ChAT+ and Som+ axons are sensitive to the onset of air-puffs, but not the duration

Mean responses to air-puffs of duration 10 ms, 30 ms, 50 ms, 100 ms, 150ms, 200 ms, 300 ms, and 500 ms in: **a**) ChAT+ axons (individial axon ROIs averged over FOVs, as in Figure 3d-e) in *oriens/alveus* (*o/a.*). **b**) Som+ axons (whole-field ROIs in *lacunosum-moleculare* (*l-m.*), as in Figure 2c-e).

Fig. S10. Imaging GCaMP6f-expressing excitatory projections to CA1

a) Injection sites of rAAV(*Synapsin-GCaMP6f*) into CA3 (left), LEC (middle), or MEC (right) ipsilateral to the imaged hemisphere of CA1. **b**) Locomotion signals in CA3, LEC, and MEC axons (whole-field ROIs). **c**) Example responses of single CA3 axons to running and air-puffs. While most CA3 axons do not respond to air-puffs, as reflected in whole-field fluorescence (Fig.. 4), a sparse subset of CA3 axons do respond, potentially providing the drive to excite a sparse subset of CA1 PCs, even though the much stronger LEC and MEC signals are being inhibited.

Fig. S11. PSEM^{89} inactivation of Som+ interneurons *in vivo*

Mean air-puff responses of Som+/PSAM^{L141F}-GlyR+ interneurons (left) and Som−/PSAM^{L141F}-GlyR− interneurons (right) in control and PSEM^{89} administration (60 mg/kg PSEM^{89} i.p. 12-30 min before stimulus presentation).

Fig. S12. Identification of pyramidal cells with significant stimulus-evoked activity

a) Histograms of positive (blue) and negative (red) deflections in the ΔF/F trace. Event amplitudes are quantified in terms of σ, which is determined for each cell and is defined as the standard deviation of the noise of the cell's ΔF/F trace. Histograms show the distribution of event durations for events greater than or equal to each σ level. **b**) False positive rates for 2-, 3-, and 4-σ events (pooled across all FOVs in all mice used in Fig. 5 and Fig. S13). False positive rate curves are calculated for each σ level by dividing the number of negative events at that level by the number of positive events at that level. See ref. *33* for more details. Event onsets are defined as the times when the ΔF/F exceeds 2-σ, and offset is defined as the time at which the ΔF/F falls below 0.5 σ. A decaying exponential was fit by least-squares to the false positive rate values,

allowing for the determination of a minimum transient duration at each σlevel for different confidence levels.

Fig. S13. Effects of local PSEM and bicuculine on PC populations
a) $PSEM^{89}$ does not alter the mean % of active cells during air-puffs (ctrl: 10.1 ± 2.6%, $PSEM^{89}$: 7.1 ± 1.3%, n=4 FOVs; paired t-test) or the duration of air-puff-evoked transients in cells active in both drug conditions (ctrl: 2.73 ± 0.2s, $PSEM^{89}$: 2.56 ± 0.2s, n = 21 cells; paired t-test) in mice that do not express $PSAM^{L141F}$-GlyR. **b**) 20 μM Bicuculine increases the mean % of active cells during air-puffs (ctrl: 7.6 ± 0.7%, Bic.: 41.3 ± 6.7%, n=13 FOVs; paired t-test) and the duration of air-puff-evoked transients in cells active in both drug conditions (ctrl: 2.72 ± 0.09 s, Bic: 3.21 ± 0.09 s, n = 114 cells; paired t-test). Bars represent mean ± s.e.m., ***p < 0.001, ns = non-significant

Fig. S14. Expression of eNpHR3.0-eGFP in CA1 Som+ interneurons
a) Left: example confocal image of eNpHR3.0-eGFP expression in dorsal CA1 of injected *Som-cre* mice. Right: Mean % of cre/tdTomato+ cells in *oriens* that are also eNpHR3.0-eGFP+. **b**) Top left: Example cell-attached recording from Som+/eNpHR3.0-eGFP+ neuron *ex vivo*, showing suppression of spontaneous spiking with 593 nm light. Bottom left: Example whole-cell current clamp recording from Som+/eNpHR3.0-eGFP+ neuron *ex vivo*, showing hyperpolarization with 593 nm laser light at two resting voltages. Right: example whole-cell current clamp recordings from Som+/eNpHR3.0-eGFP+ neuron *ex vivo*, with overlapping laser light and current injection.

Fig. S15. Hypothesized conceptual model of CFC
a) Schematic of sensory processing in the case of fear conditioning to a unimodal CS, such as a tone. **b**) Schematic of sensory processing in the case of fear conditioning to a multimodal contextual CS, which requires the hippocampus to form a unified respresentation of the context from disparate sensory cues. **c**) Traditional view of CFC. The hippocampus processes the context CS independent of the sensory features of the US. **d**) We propose an alternative conceptual model of CFC. Sensory information about the US can reach CA1 through direct inputs from the entorhinal cortex, requiring active filtering. The US also sends parallel signals to the medial septum cholinergic system, which excites CA1 dendrite-targeting interneurons to prevent US signals from influencing hippocampal CS processing.

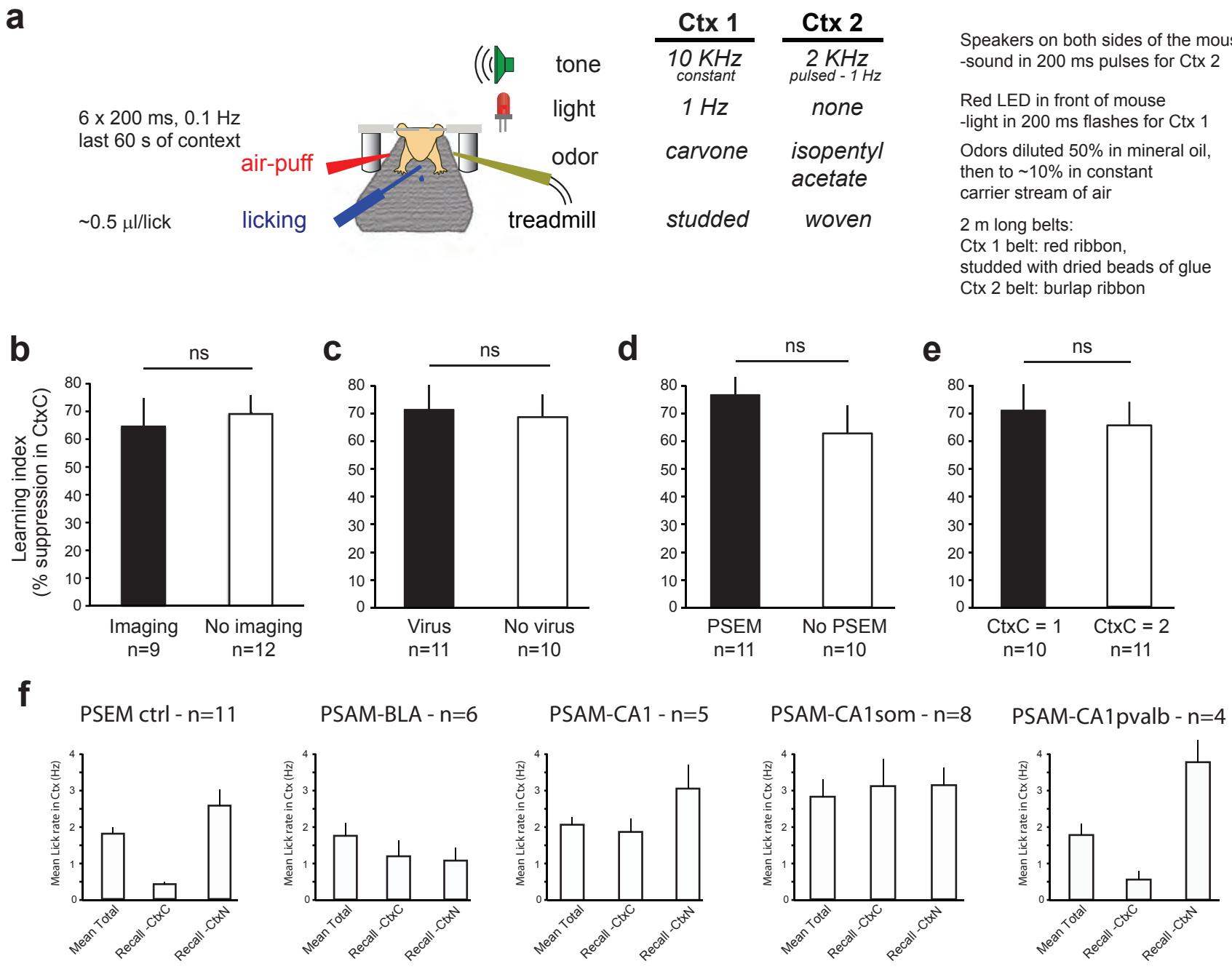

Supplementary Figure 1
Lovett-Barron et al.

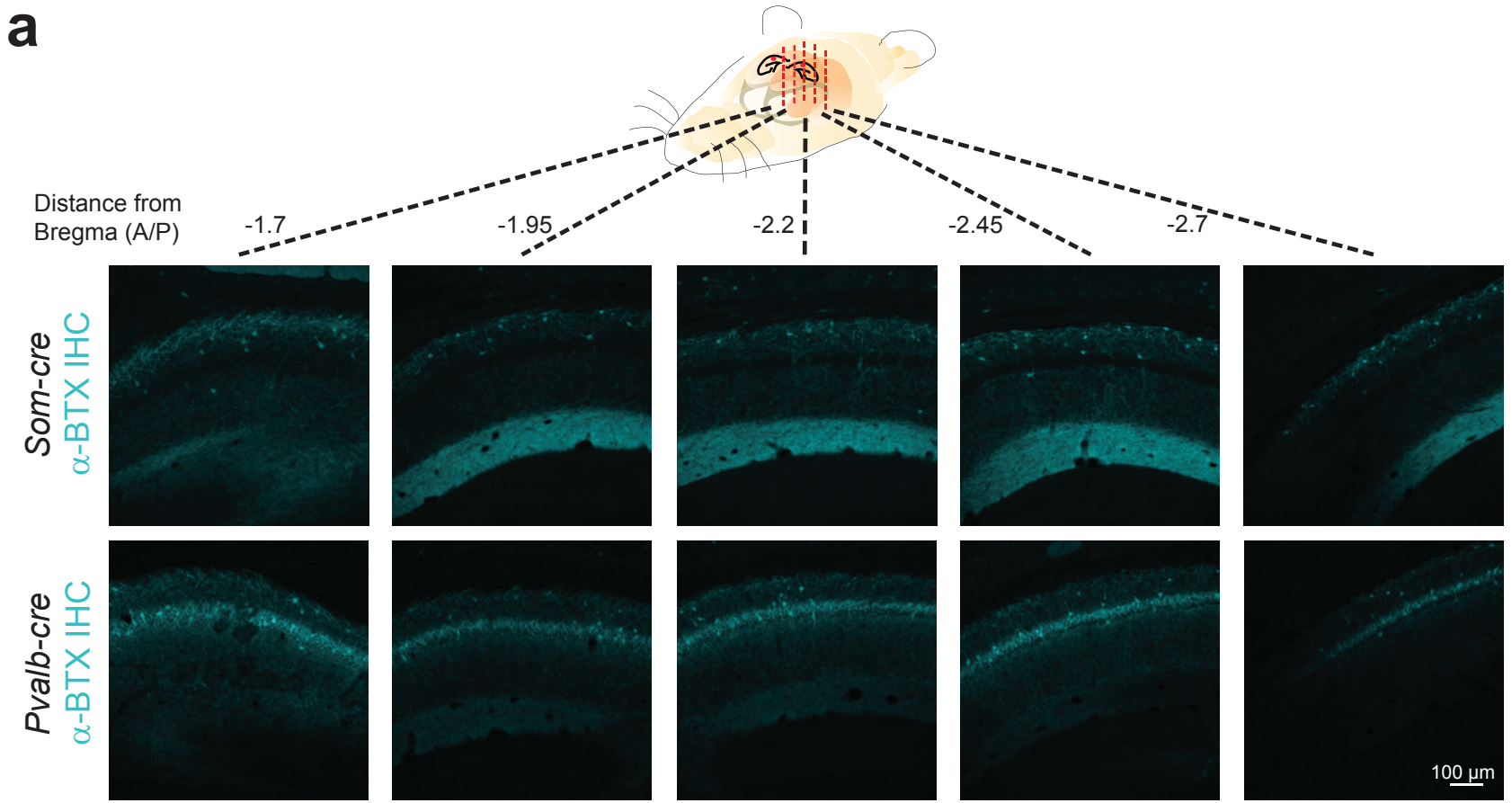

Supplementary Figure 2
Lovett-Barron et al.

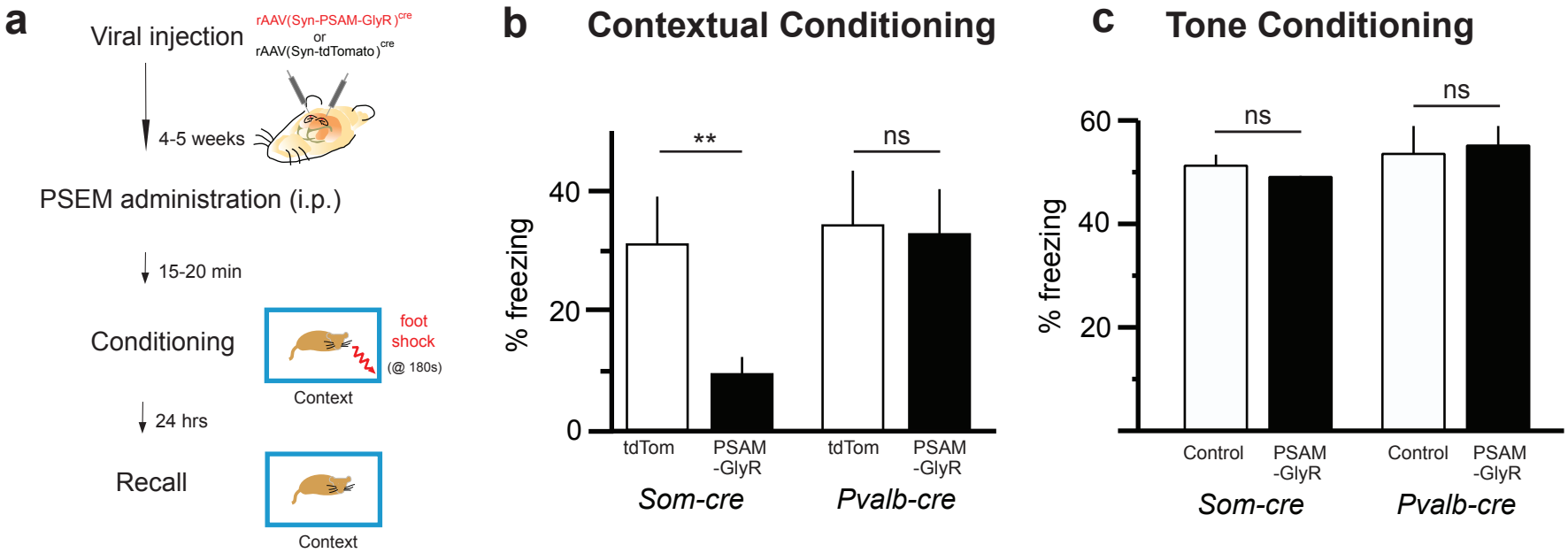

Supplementary Figure 3
Lovett-Barron et al.

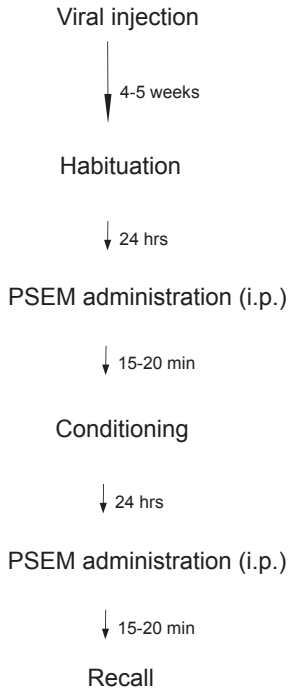

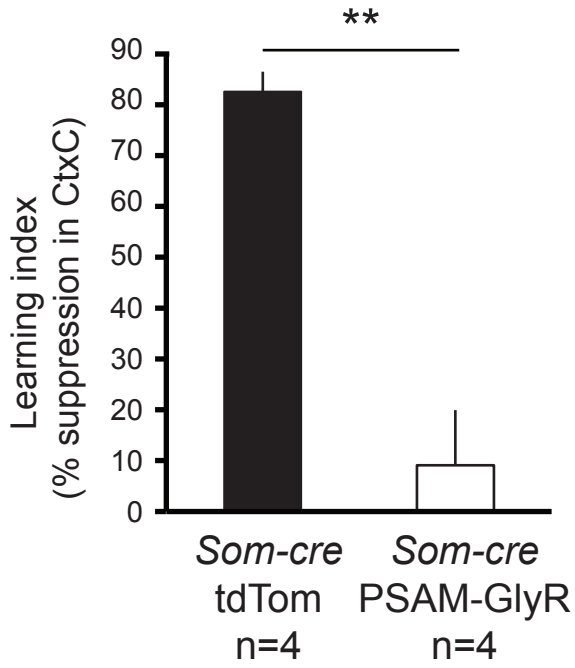

Supplementary Figure 4
Lovett-Barron et al.

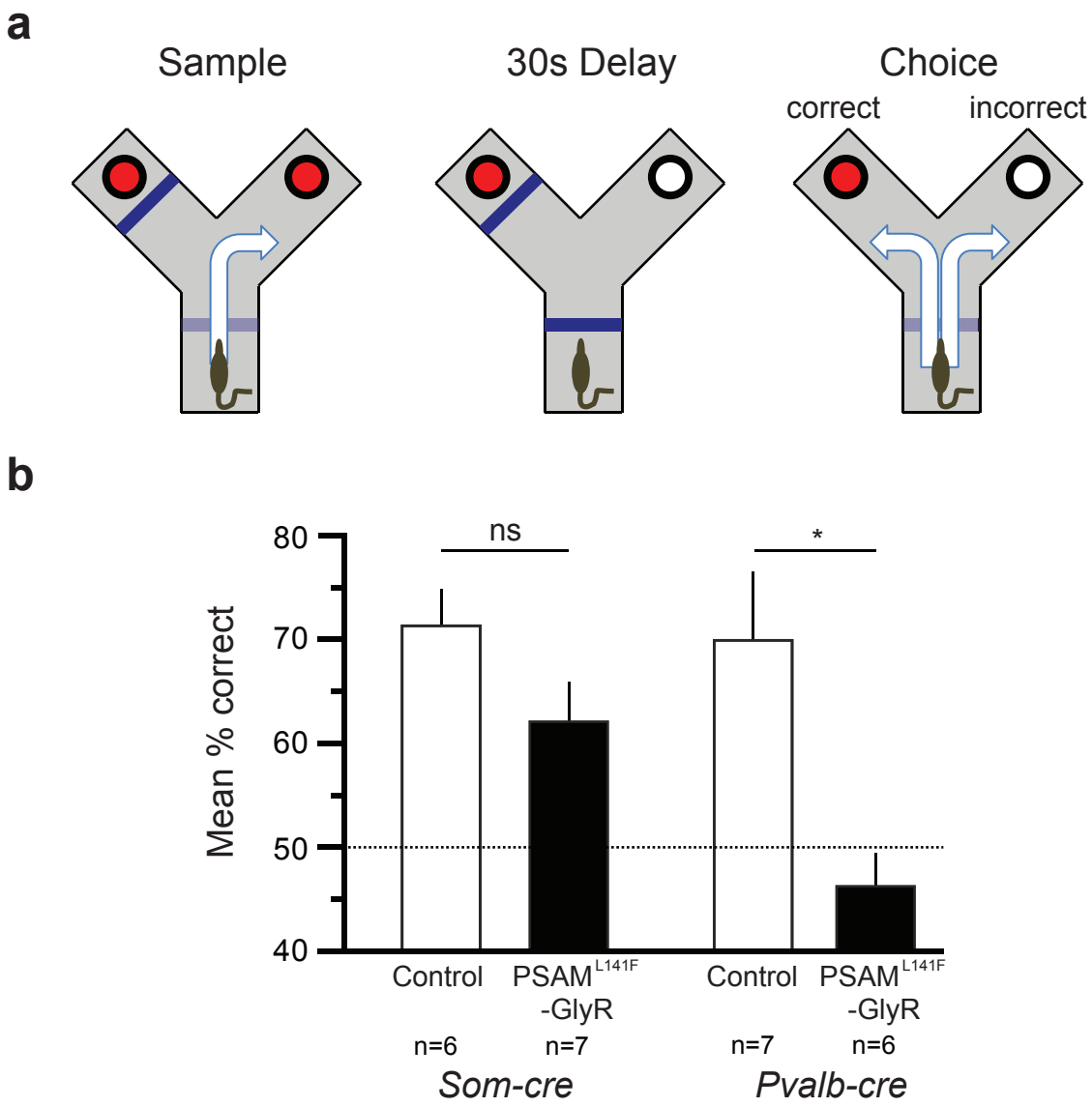

Supplementary Figure 5
Lovett-Barron et al.

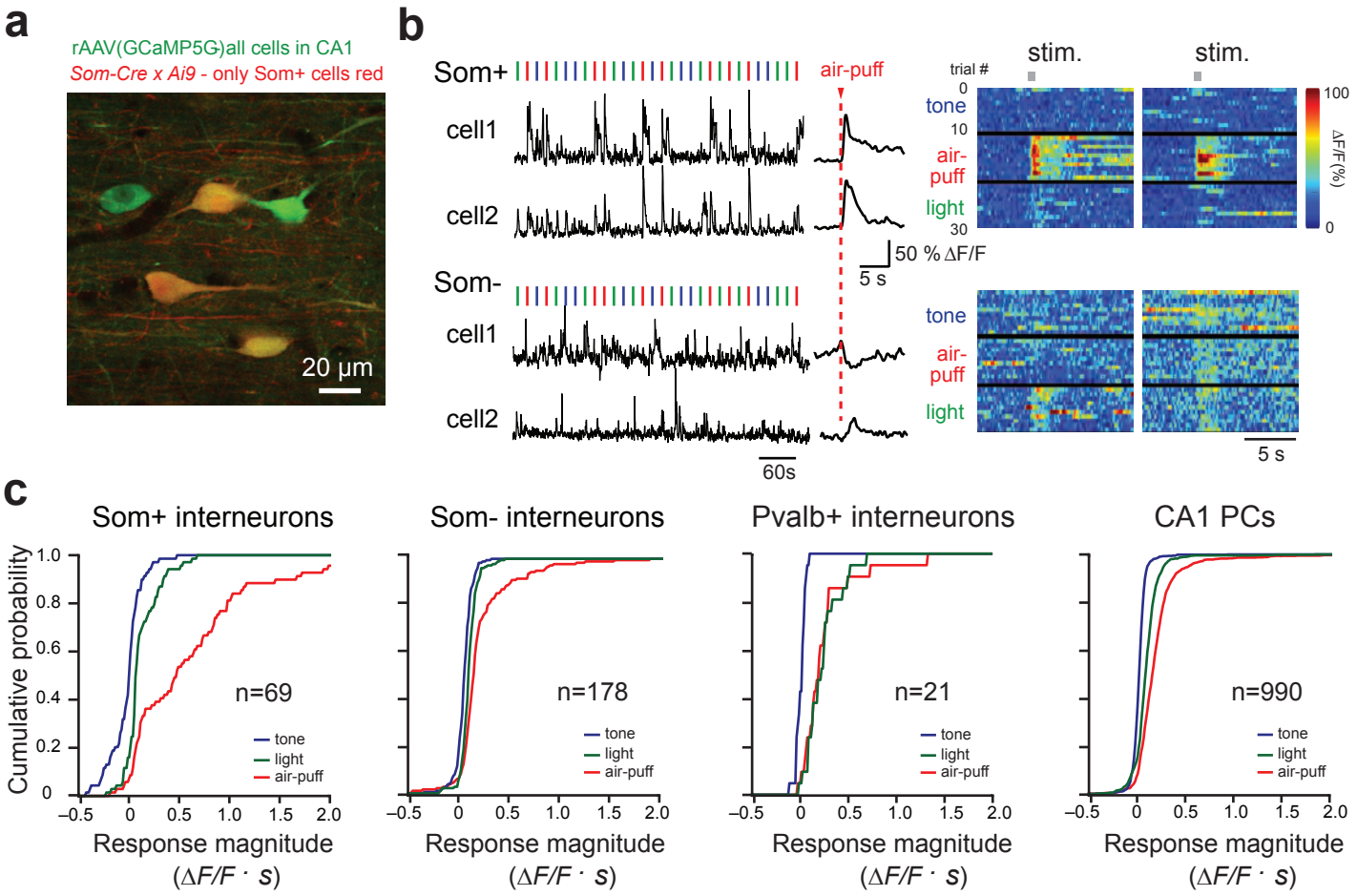

Supplementary Figure 6
Lovett-Barron et al.

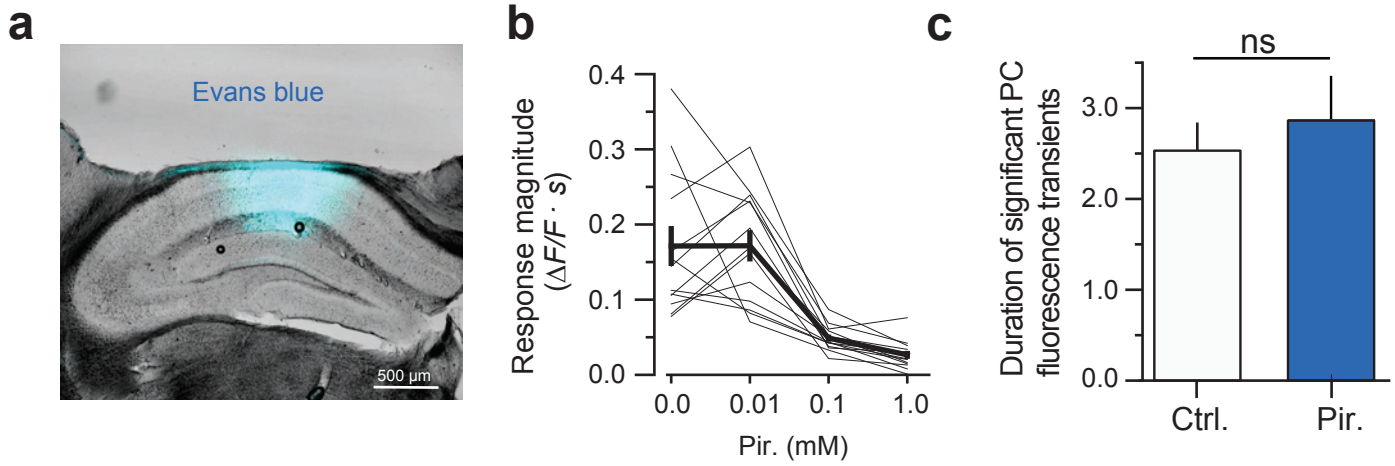

Supplementary Figure 7
Lovett-Barron et al.

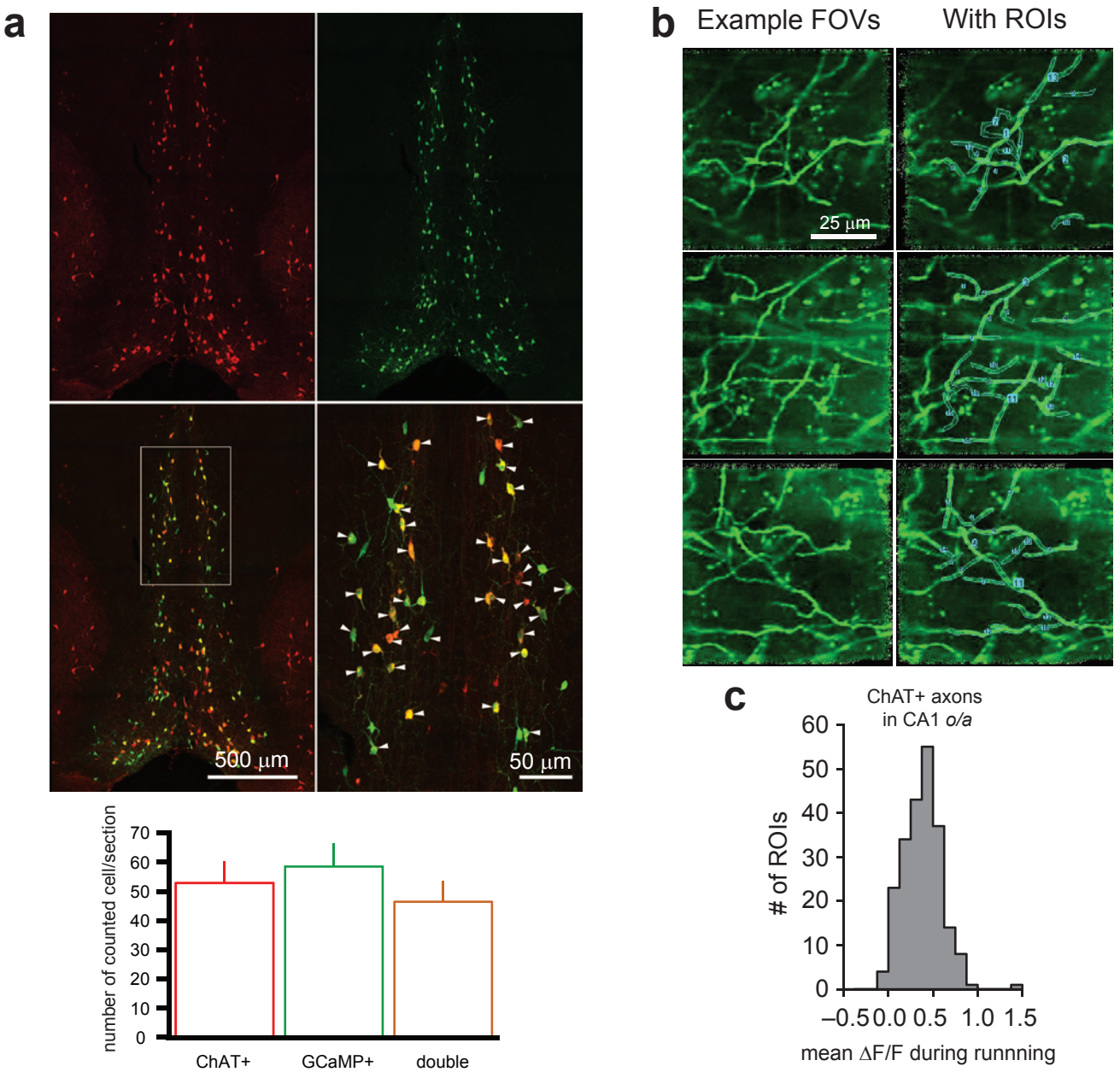

Supplementary Figure 8
Lovett-Barron et al.

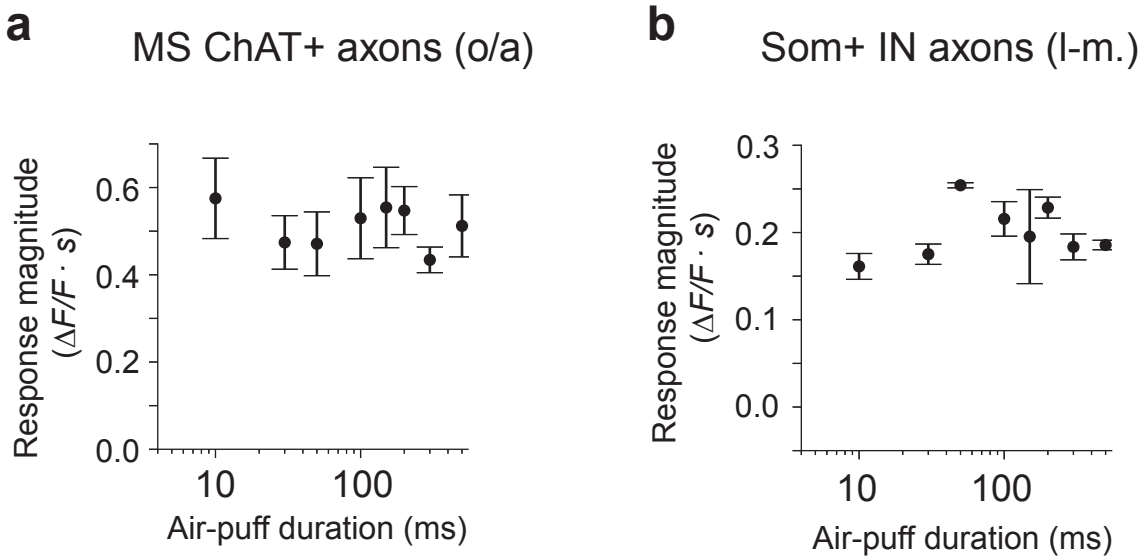

Supplementary Figure 9
Lovett-Barron et al.

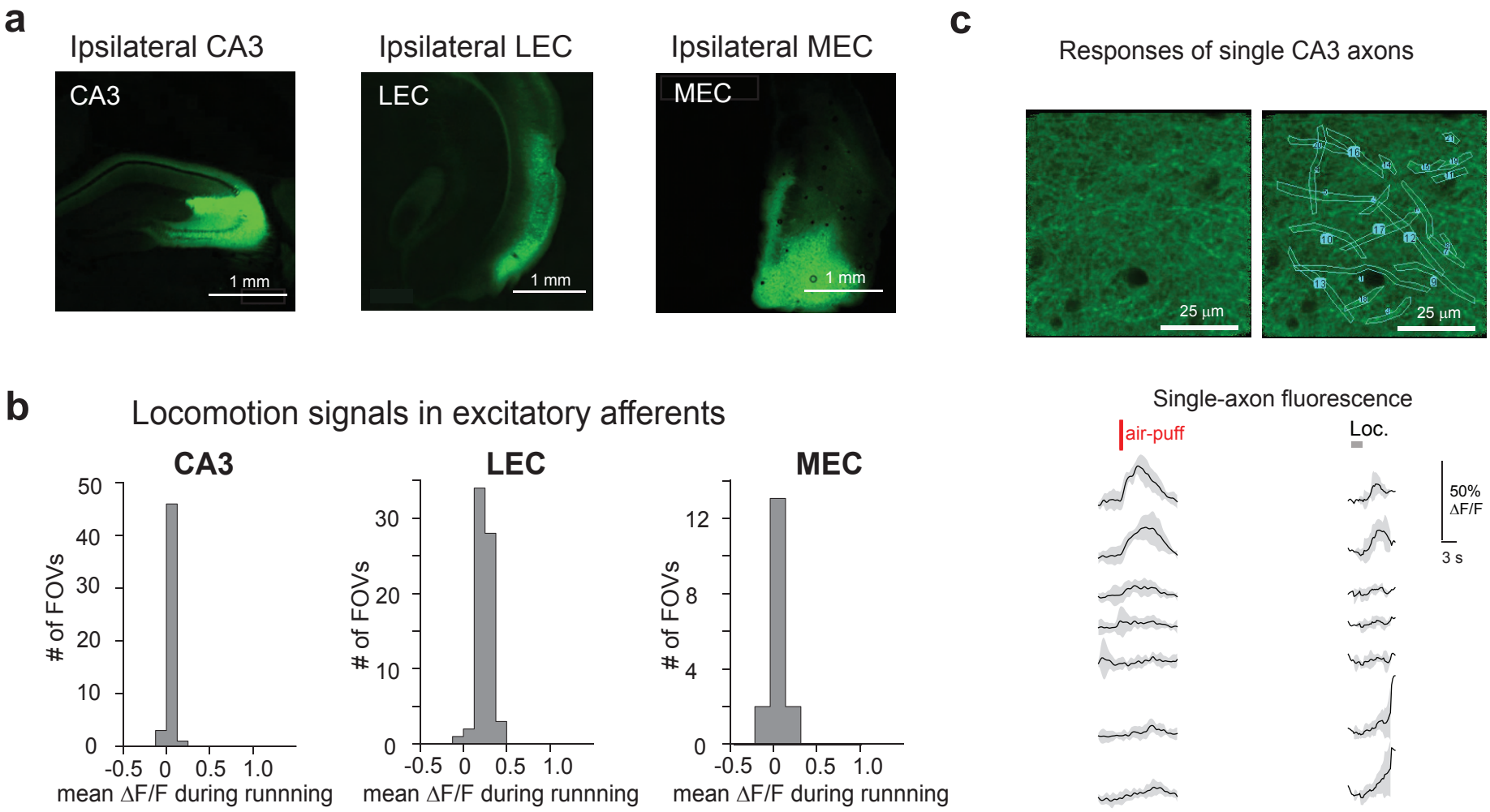

Supplementary Figure 10
Lovett-Barron et al.

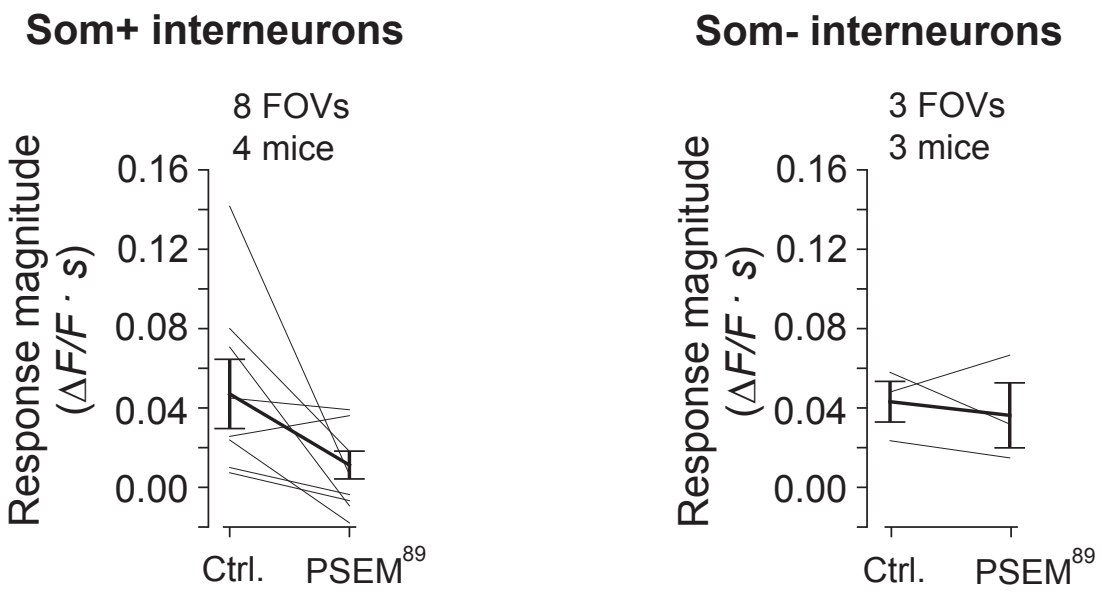

Supplementary Figure 11
Lovett-Barron et al.

a

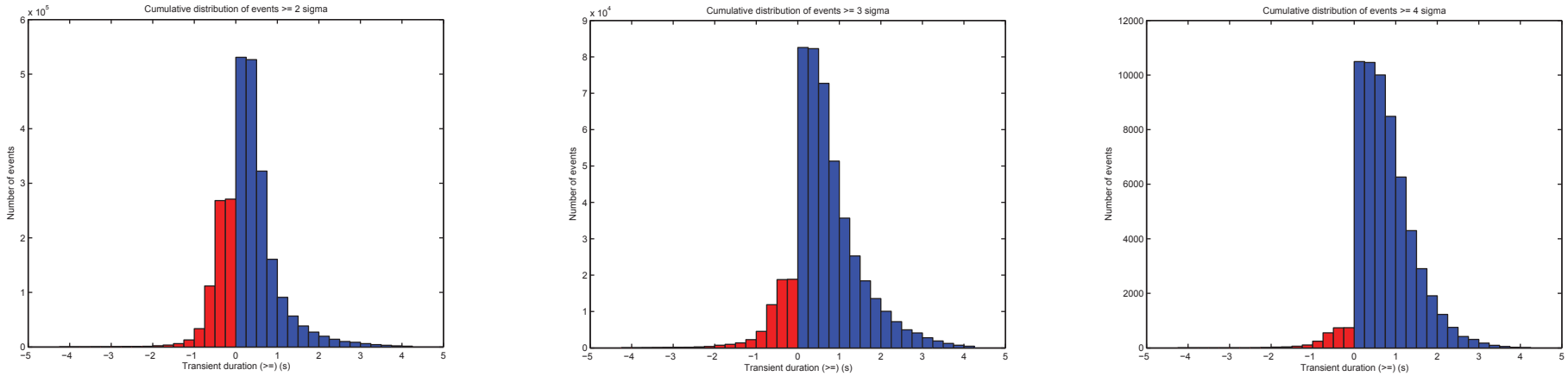

b

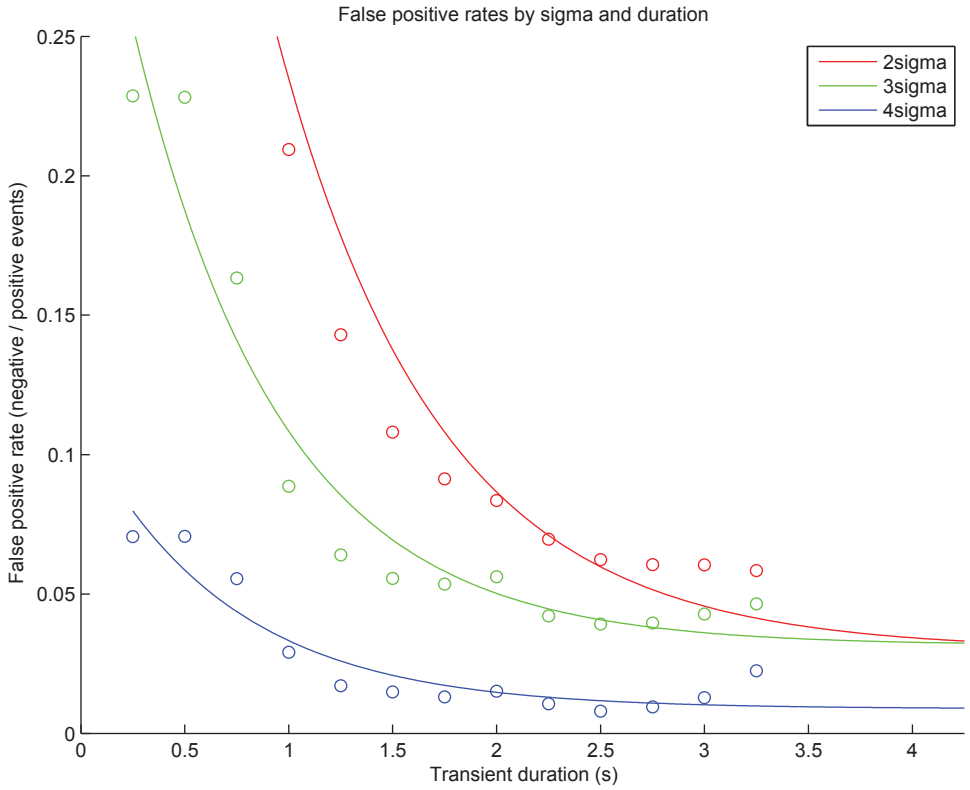

Supplementary Figure 12
Lovett-Barron et al.

a Effect of local PSEM^{89} on PCs in *Som-cre* mice not expressing PSAM^{L141F}-GlyR

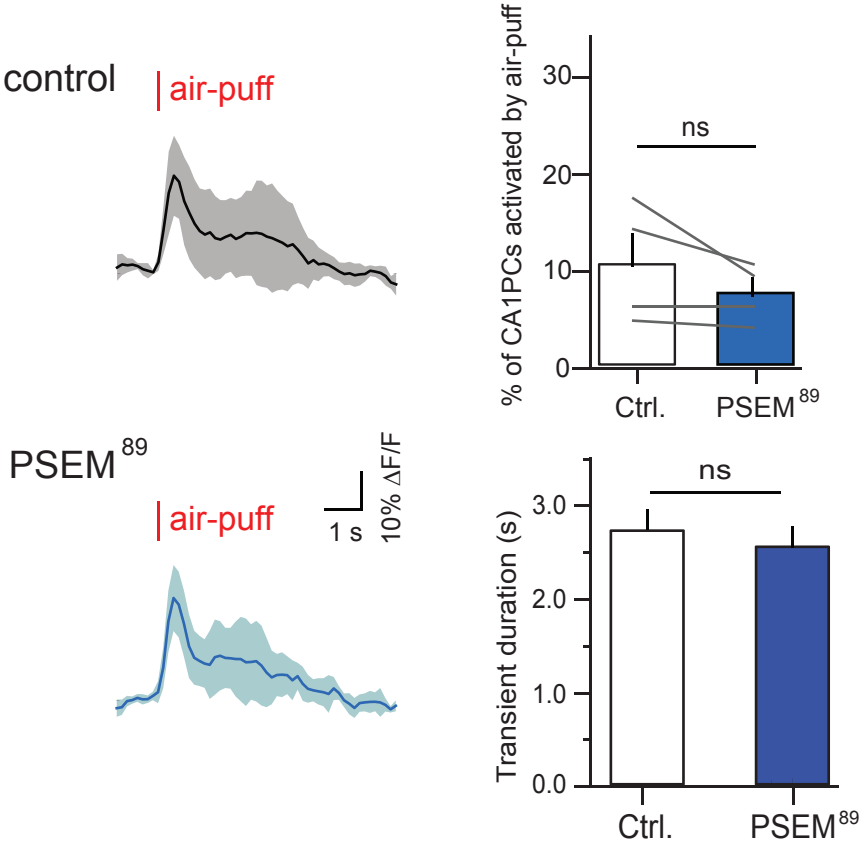

b Effect of local GABA$_A$R block (20 μM bicuculine) on PCs

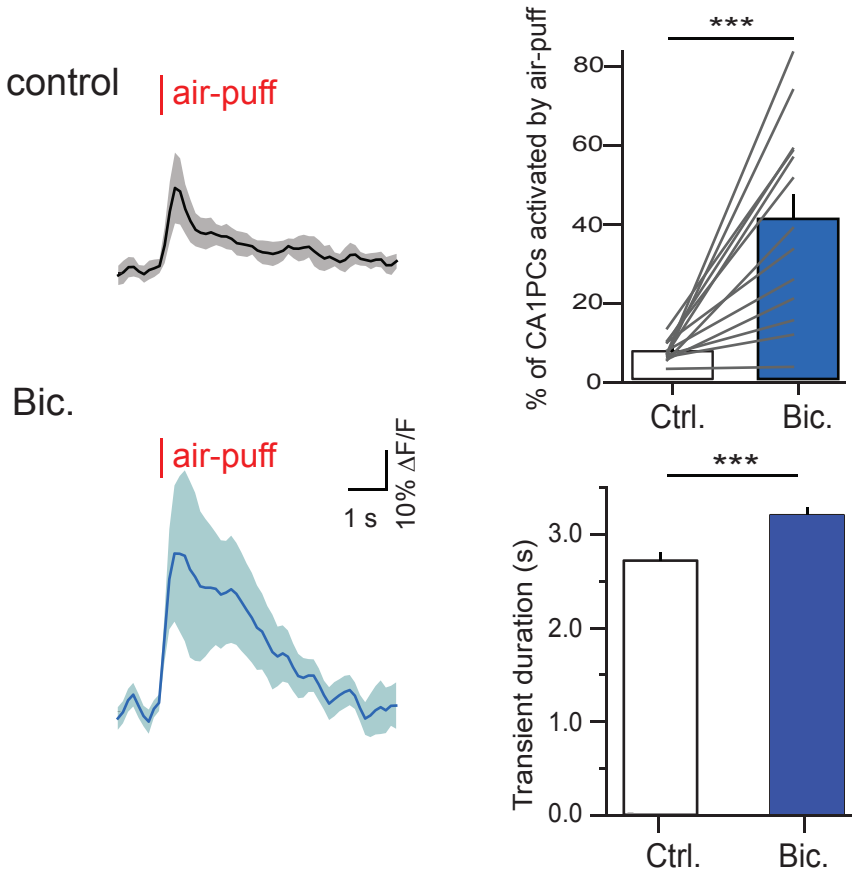

Supplementary Figure 13
Lovett-Barron et al.

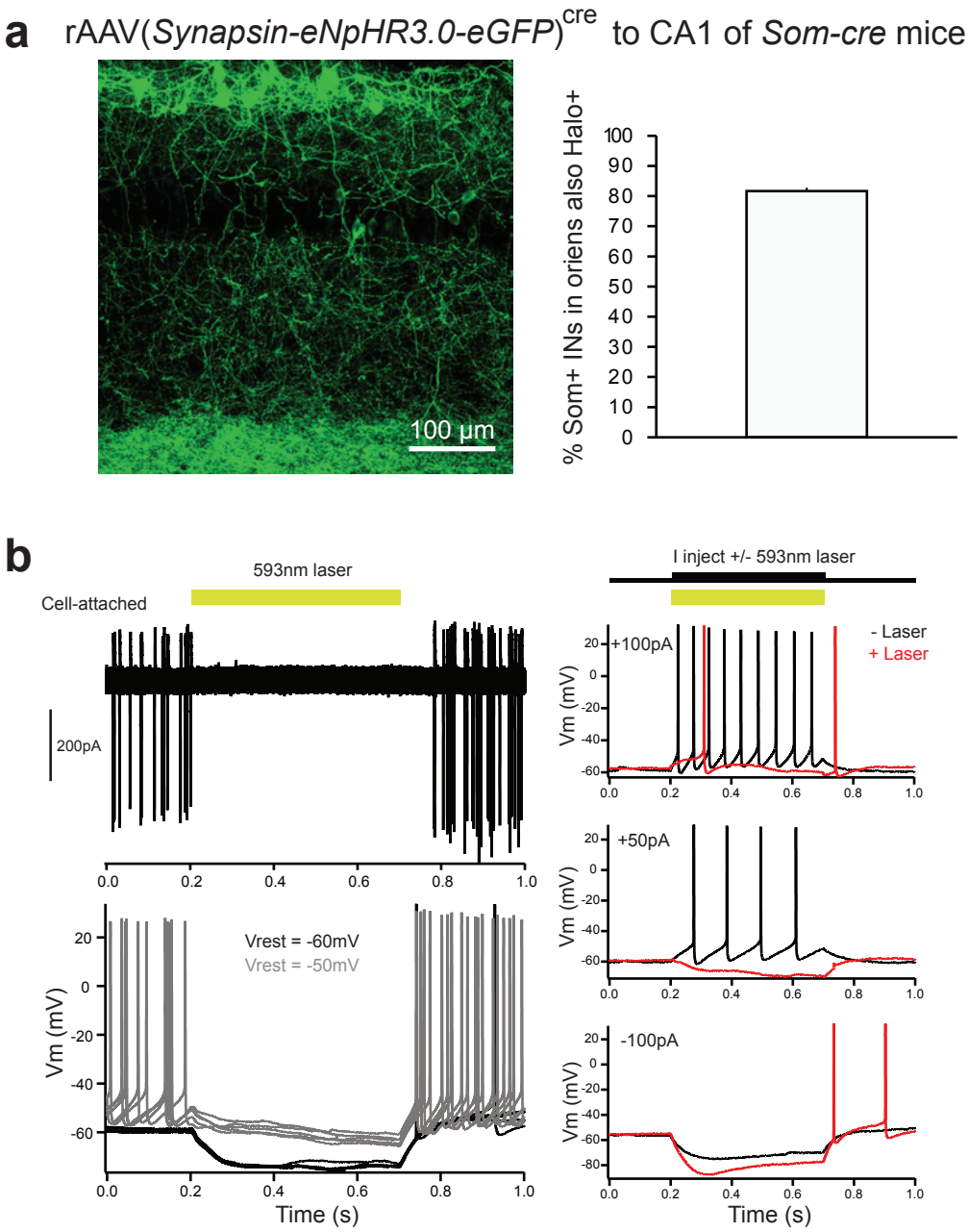

Supplementary Figure 14
Lovett-Barron et al.

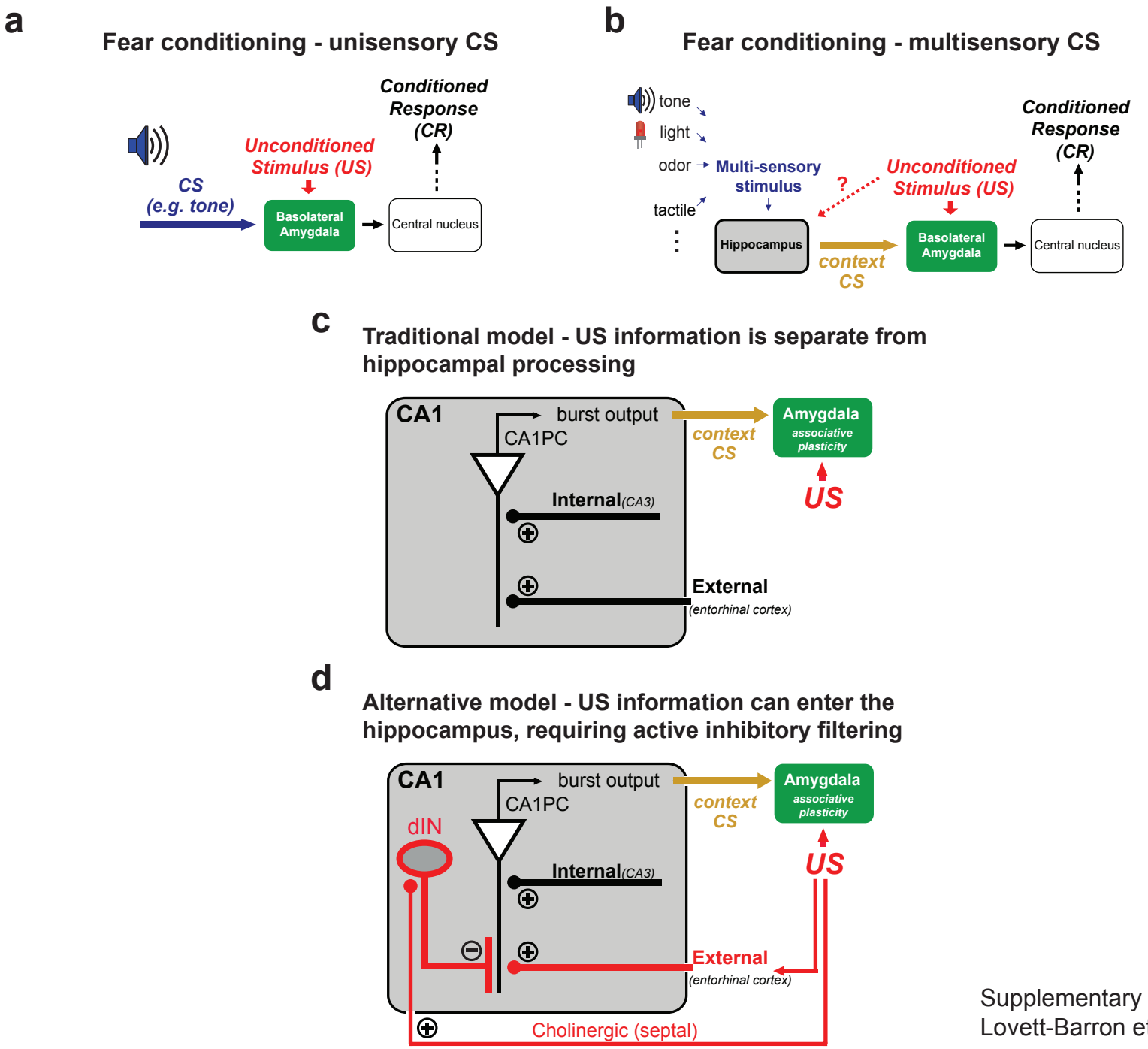

Supplementary Figure 15
Lovett-Barron et al.

References

1. M. S. Fanselow, Associative vs. topographical accounts of the immediate shock freezing deficit in rats: Implications for the response selection rules governing species specific defensive reactions. *Learn*. *Motiv*. **17**, 16–39 (1986). doi:10.1016/0023-9690(86)90018-4

2. M. S. Fanselow, Factors governing one trial contextual conditioning. *Anim*. *Learn*. *Behav*. **18**, 264–270 (1990). doi:10.3758/BF03205285

3. S. Maren, Neurobiology of Pavlovian fear conditioning. *Annu*. *Rev*. *Neurosci*. **24**, 897–931 (2001). doi:10.1146/annurev.neuro.24.1.897 Medline

4. J. W. Rudy, N. C. Huff, P. Matus-Amat, Understanding contextual fear conditioning: insights from a two-process model. *Neurosci*. *Biobehav*. *Rev*. **28**, 675–685 (2004). doi:10.1016/j.neubiorev.2004.09.004 Medline

5. M. S. Fanselow, A. M. Poulos, The neuroscience of mammalian associative learning. *Annu*. *Rev*. *Psychol*. **56**, 207–234 (2005). doi:10.1146/annurev.psych.56.091103.070213 Medline

6. J. J. Kim, M. S. Fanselow, Modality-specific retrograde amnesia of fear. *Science* **256**, 675–677 (1992). doi:10.1126/science.1585183 Medline

7. R. G. Phillips, J. E. LeDoux, Differential contribution of amygdala and hippocampus to cued and contextual fear conditioning. *Behav*. *Neurosci*. **106**, 274–285 (1992). doi:10.1037/0735-7044.106.2.274 Medline

8. S. L. Young, D. L. Bohenek, M. S. Fanselow, NMDA processes mediate anterograde amnesia of contextual fear conditioning induced by hippocampal damage: immunization against amnesia by context preexposure. *Behav*. *Neurosci*. **108**, 19–29 (1994). doi:10.1037/0735-7044.108.1.19 Medline

9. S. Maren, M. S. Fanselow, Synaptic plasticity in the basolateral amygdala induced by hippocampal formation stimulation in vivo. *J*. *Neurosci*. **15**, 7548–7564 (1995). Medline

10. P. W. Frankland, S. A. Josselyn, S. G. Anagnostaras, J. H. Kogan, E. Takahashi, A. J. Silva, Consolidation of CS and US representations in associative fear conditioning. *Hippocampus* **14**, 557–569 (2004). doi:10.1002/hipo.10208 Medline

11. M. S. Fanselow, J. P. DeCola, S. L. Young, Mechanisms responsible for reduced contextual conditioning with massed unsignaled unconditional stimuli. *J*. *Exp*. *Psychol*. *Anim*. *Behav*. *Process*. **19**, 121–137 (1993). doi:10.1037/0097-7403.19.2.121 Medline

12. P. Sah, E. S. Faber, M. Lopez De Armentia, J. Power, The amygdaloid complex: anatomy and physiology. *Physiol*. *Rev*. **83**, 803–834 (2003). Medline

13. O. J. Ahmed, M. R. Mehta, The hippocampal rate code: Anatomy, physiology and theory. *Trends Neurosci*. **32**, 329–338 (2009). doi:10.1016/j.tins.2009.01.009 Medline

14. R. P. Kesner, Behavioral functions of the CA3 subregion of the hippocampus. *Learn*. *Mem*. **14**, 771–781 (2007). doi:10.1101/lm.688207 Medline

15. S. Maren, M. S. Fanselow, Electrolytic lesions of the fimbria/fornix, dorsal hippocampus, or entorhinal cortex produce anterograde deficits in contextual fear conditioning in rats. *Neurobiol*. *Learn*. *Mem*. **67**, 142–149 (1997). doi:10.1006/nlme.1996.3752 Medline

16. N. L. Golding, N. P. Staff, N. Spruston, Dendritic spikes as a mechanism for cooperative long-term potentiation. *Nature* **418**, 326–331 (2002). doi:10.1038/nature00854 Medline

17. J. T. Dudman, D. Tsay, S. A. Siegelbaum, A role for synaptic inputs at distal dendrites: instructive signals for hippocampal long-term plasticity. *Neuron* **56**, 866–879 (2007). doi:10.1016/j.neuron.2007.10.020 Medline

18. H. Takahashi, J. C. Magee, Pathway interactions and synaptic plasticity in the dendritic tuft regions of CA1 pyramidal neurons. *Neuron* **62**, 102–111 (2009). doi:10.1016/j.neuron.2009.03.007 Medline

19. M. W. Jones, M. A. Wilson, Theta rhythms coordinate hippocampal-prefrontal interactions in a spatial memory task. *PLoS Biol*. **3**, e402 (2005). doi:10.1371/journal.pbio.0030402 Medline

20. K. D. Harris, H. Hirase, X. Leinekugel, D. A. Henze, G. Buzsáki, Temporal interaction between single spikes and complex spike bursts in hippocampal pyramidal cells. *Neuron* **32**, 141–149 (2001). doi:10.1016/S0896-6273(01)00447-0 Medline

21. W. Xu, W. Morishita, P. S. Buckmaster, Z. P. Pang, R. C. Malenka, T. C. Südhof, Distinct neuronal coding schemes in memory revealed by selective erasure of fast synchronous synaptic transmission. *Neuron* **73**, 990–1001 (2012). doi:10.1016/j.neuron.2011.12.036 Medline

22. T. F. Freund, G. Buzsáki, Interneurons of the hippocampus. *Hippocampus* **6**, 347–470 (1996). doi:10.1002/(SICI)1098-1063(1996)6:4<347::AID-HIPO1>3.0.CO;2-I Medline

23. T. Klausberger, P. Somogyi, Neuronal diversity and temporal dynamics: The unity of hippocampal circuit operations. *Science* **321**, 53–57 (2008). doi:10.1126/science.1149381 Medline

24. A. Losonczy, B. V. Zemelman, A. Vaziri, J. C. Magee, Network mechanisms of theta related neuronal activity in hippocampal CA1 pyramidal neurons. *Nat*. *Neurosci*. **13**, 967–972 (2010). doi:10.1038/nn.2597 Medline

25. M. Lovett-Barron, G. F. Turi, P. Kaifosh, P. H. Lee, F. Bolze, X. H. Sun, J. F. Nicoud, B. V. Zemelman, S. M. Sternson, A. Losonczy, Regulation of neuronal input transformations by tunable dendritic inhibition. *Nat*. *Neurosci*. **15**, 423–430, S1–S3 (2012). doi:10.1038/nn.3024 Medline

26. S. Royer, B. V. Zemelman, A. Losonczy, J. Kim, F. Chance, J. C. Magee, G. Buzsáki, Control of timing, rate and bursts of hippocampal place cells by dendritic and somatic inhibition. *Nat*. *Neurosci*. **15**, 769–775 (2012). doi:10.1038/nn.3077 Medline

27. W. J. Mahoney, J. J. B. Ayres, One-trial simultaneous and backward fear conditioning as reflected in conditioned suppression of licking in rats. *Anim*. *Learn*. *Behav*. **4**, 357–362 (1976). doi:10.3758/BF03214421

28. M. E. Bouton, R. C. Bolles, Conditioned fear assessed by freezing and by the suppression of three different baselines. *Anim*. *Learn*. *Behav*. **8**, 429–434 (1980). doi:10.3758/BF03199629

29. P. Kaifosh, M. Lovett-Barron, G. F. Turi, T. R. Reardon, A. Losonczy, Septo-hippocampal GABAergic signaling across multiple modalities in awake mice. *Nat*. *Neurosci*. **16**, 1182–1184 (2013). doi:10.1038/nn.3482 Medline

30. C. J. Magnus, P. H. Lee, D. Atasoy, H. H. Su, L. L. Looger, S. M. Sternson, Chemical and genetic engineering of selective ion channel-ligand interactions. *Science* **333**, 1292–1296 (2011). doi:10.1126/science.1206606 Medline

31. S. G. Anagnostaras, G. D. Gale, M. S. Fanselow, Hippocampus and contextual fear conditioning: recent controversies and advances. *Hippocampus* **11**, 8–17 (2001). doi:10.1002/1098-1063(2001)11:1<8::AID-HIPO1015>3.0.CO;2-7 Medline

32. I. Goshen, M. Brodsky, R. Prakash, J. Wallace, V. Gradinaru, C. Ramakrishnan, K. Deisseroth, Dynamics of retrieval strategies for remote memories. *Cell* **147**, 678–689 (2011). doi:10.1016/j.cell.2011.09.033 Medline

33. A. J. Murray, J. F. Sauer, G. Riedel, C. McClure, L. Ansel, L. Cheyne, M. Bartos, W. Wisden, P. Wulff, Parvalbumin-positive CA1 interneurons are required for spatial working but not for reference memory. *Nat*. *Neurosci*. **14**, 297–299 (2011). doi:10.1038/nn.2751 Medline

34. J. Akerboom, T. W. Chen, T. J. Wardill, L. Tian, J. S. Marvin, S. Mutlu, N. C. Calderón, F. Esposti, B. G. Borghuis, X. R. Sun, A. Gordus, M. B. Orger, R. Portugues, F. Engert, J. J. Macklin, A. Filosa, A. Aggarwal, R. A. Kerr, R. Takagi, S. Kracun, E. Shigetomi, B. S. Khakh, H. Baier, L. Lagnado, S. S. Wang, C. I. Bargmann, B. E. Kimmel, V. Jayaraman, K. Svoboda, D. S. Kim, E. R. Schreiter, L. L. Looger, Optimization of a GCaMP calcium indicator for neural activity imaging. *J*. *Neurosci*. **32**, 13819–13840 (2012). doi:10.1523/JNEUROSCI.2601-12.2012 Medline

35. D. A. Dombeck, C. D. Harvey, L. Tian, L. L. Looger, D. W. Tank, Functional imaging of hippocampal place cells at cellular resolution during virtual navigation. *Nat*. *Neurosci*. **13**, 1433–1440 (2010). doi:10.1038/nn.2648 Medline

36. D. A. Dombeck, A. N. Khabbaz, F. Collman, T. L. Adelman, D. W. Tank, Imaging large-scale neural activity with cellular resolution in awake, mobile mice. *Neuron* **56**, 43–57 (2007). doi:10.1016/j.neuron.2007.08.003 Medline

37. O. Herreras, J. M. Solís, M. D. Muñoz, R. Martín del Río, J. Lerma, Sensory modulation of hippocampal transmission. I. Opposite effects on CA1 and dentate gyrus synapsis. *Brain Res*. **461**, 290–302 (1988). doi:10.1016/0006-8993(88)90259-4 Medline

38. S. Khanna, Dorsal hippocampus field CA1 pyramidal cell responses to a persistent versus an acute nociceptive stimulus and their septal modulation. *Neuroscience* **77**, 713–721 (1997). doi:10.1016/S0306-4522(96)00456-3 Medline

39. M. Funahashi, Y. F. He, T. Sugimoto, R. Matsuo, Noxious tooth pulp stimulation suppresses c-fos expression in the rat hippocampal formation. *Brain Res*. **827**, 215–220 (1999). doi:10.1016/S0006-8993(99)01250-0 Medline

40. O. S. Vinogradova, Hippocampus as comparator: Role of the two input and two output systems of the hippocampus in selection and registration of information. *Hippocampus* **11**, 578–598 (2001). doi:10.1002/hipo.1073 Medline

41. J. J. Lawrence, J. M. Statland, Z. M. Grinspan, C. J. McBain, Cell type-specific dependence of muscarinic signalling in mouse hippocampal stratum oriens interneurones. *J*. *Physiol*. **570**, 595–610 (2006). doi:10.1113/jphysiol.2005.100875 Medline

42. R. N. Leão, S. Mikulovic, K. E. Leão, H. Munguba, H. Gezelius, A. Enjin, K. Patra, A. Eriksson, L. M. Loew, A. B. Tort, K. Kullander, OLM interneurons differentially modulate CA3 and entorhinal inputs to hippocampal CA1 neurons. *Nat*. *Neurosci*. **15**, 1524–1530 (2012). doi:10.1038/nn.3235 Medline

43. S. W. Miller, P. M. Groves, Sensory evoked neuronal activity in the hippocampus before and after lesions of the medial septal nuclei. *Physiol*. *Behav*. **18**, 141–146 (1977). doi:10.1016/0031-9384(77)90106-8 Medline

44. O. Herreras, J. M. Solís, A. S. Herranz, R. M. del Río, J. Lerma, Sensory modulation of hippocampal transmission. II. Evidence for a cholinergic locus of inhibition in the Schaffer-CA1 synapse. *Brain Res*. **461**, 303–313 (1988). doi:10.1016/0006-8993(88)90260-0 Medline

45. F. Zheng, S. Khanna, Selective destruction of medial septal cholinergic neurons attenuates pyramidal cell suppression, but not excitation in dorsal hippocampus field CA1 induced by subcutaneous injection of formalin. *Neuroscience* **103**, 985–998 (2001). doi:10.1016/S0306-4522(01)00006-9 Medline

46. J. J. Letzkus, S. B. Wolff, E. M. Meyer, P. Tovote, J. Courtin, C. Herry, A. Lüthi, A disinhibitory microcircuit for associative fear learning in the auditory cortex. *Nature* **480**, 331–335 (2011). doi:10.1038/nature10674 Medline

47. H. Widmer, L. Ferrigan, C. H. Davies, S. R. Cobb, Evoked slow muscarinic acetylcholinergic synaptic potentials in rat hippocampal interneurons. *Hippocampus* **16**, 617–628 (2006). doi:10.1002/hipo.20191 Medline

48. G. D. Gale, S. G. Anagnostaras, M. S. Fanselow, Cholinergic modulation of pavlovian fear conditioning: effects of intrahippocampal scopolamine infusion. *Hippocampus* **11**, 371–376 (2001). doi:10.1002/hipo.1051 Medline

49. S. Dasari, A. T. Gulledge, M1 and M4 receptors modulate hippocampal pyramidal neurons. *J*. *Neurophysiol*. **105**, 779–792 (2011). doi:10.1152/jn.00686.2010 Medline

50. M. E. Hasselmo, The role of acetylcholine in learning and memory. *Curr*. *Opin*. *Neurobiol*. **16**, 710–715 (2006). doi:10.1016/j.conb.2006.09.002 Medline

51. L. Calandreau, R. Jaffard, A. Desmedt, Dissociated roles for the lateral and medial septum in elemental and contextual fear conditioning. *Learn*. *Mem*. **14**, 422–429 (2007). doi:10.1101/lm.531407 Medline

52. T.-W. Chen, T. J. Wardill, Y. Sun, S. R. Pulver, S. L. Renninger, A. Baohan, E. R. Schreiter, R. A. Kerr, M. B. Orger, V. Jayaraman, L. L. Looger, K. Svoboda, D. S. Kim, Ultrasensitive fluorescent proteins for imaging neuronal activity. *Nature* **499**, 295–300 (2013). doi:10.1038/nature12354 Medline

53. E. L. Hargreaves, G. Rao, I. Lee, J. J. Knierim, Major dissociation between medial and lateral entorhinal input to dorsal hippocampus. *Science* **308**, 1792–1794 (2005). doi:10.1126/science.1110449 Medline

54. S. J. Zhang, J. Ye, C. Miao, A. Tsao, I. Cerniauskas, D. Ledergerber, M. B. Moser, E. I. Moser, Optogenetic dissection of entorhinal-hippocampal functional connectivity. *Science* **340**, 1232627 (2013). doi:10.1126/science.1232627 Medline

55. L. Palmer, M. Murayama, M. Larkum, Inhibitory regulation of dendritic activity in vivo. *Frontiers in Neural Circuits* **6**, 26 (2012). doi:10.3389/fncir.2012.00026 Medline

56. F. Zhang, L. P. Wang, M. Brauner, J. F. Liewald, K. Kay, N. Watzke, P. G. Wood, E. Bamberg, G. Nagel, A. Gottschalk, K. Deisseroth, Multimodal fast optical interrogation of neural circuitry. *Nature* **446**, 633–639 (2007). doi:10.1038/nature05744 Medline

57. L. M. Romanski, J. E. LeDoux, Information cascade from primary auditory cortex to the amygdala: corticocortical and corticoamygdaloid projections of temporal cortex in the rat. *Cereb*. *Cortex* **3**, 515–532 (1993). doi:10.1093/cercor/3.6.515 Medline

58. E. Lanuza, K. Nader, J. E. Ledoux, Unconditioned stimulus pathways to the amygdala: effects of posterior thalamic and cortical lesions on fear conditioning. *Neuroscience* **125**, 305–315 (2004). doi:10.1016/j.neuroscience.2003.12.034 Medline

59. J. Brankačk, G. Buzsáki, Hippocampal responses evoked by tooth pulp and acoustic stimulation: depth profiles and effect of behavior. *Brain Res*. **378**, 303–314 (1986). doi:10.1016/0006-8993(86)90933-9 Medline

60. R. D. Burwell, D. G. Amaral, Cortical afferents of the perirhinal, postrhinal, and entorhinal cortices of the rat. *J*. *Comp*. *Neurol*. **398**, 179–205 (1998). doi:10.1002/(SICI)1096-9861(19980824)398:2<179::AID-CNE3>3.0.CO;2-Y Medline

61. S. Melzer, M. Michael, A. Caputi, M. Eliava, E. C. Fuchs, M. A. Whittington, H. Monyer, Long-range-projecting GABAergic neurons modulate inhibition in hippocampus and entorhinal cortex. *Science* **335**, 1506–1510 (2012). doi:10.1126/science.1217139 Medline

62. M. A. Moita, S. Rosis, Y. Zhou, J. E. LeDoux, H. T. Blair, Putting fear in its place: remapping of hippocampal place cells during fear conditioning. *J*. *Neurosci*. **24**, 7015–7023 (2004). doi:10.1523/JNEUROSCI.5492-03.2004 Medline

63. C. I. Bargmann, Beyond the connectome: How neuromodulators shape neural circuits. *Bioessays* **34**, 458–465 (2012) Supplementary References. doi:10.1002/bies.201100185 Medline

64. C. McClure, K. L. Cole, P. Wulff, M. Klugmann, A. J. Murray, Production and titering of recombinant adeno-associated viral vectors. *J*. *Vis*. *Exp*. **57**, e3348 (2011). 10.3791/3348 Medline

65. M. A. Kheirbek, L. J. Drew, N. S. Burghardt, D. O. Costantini, L. Tannenholz, S. E. Ahmari, H. Zeng, A. A. Fenton, R. Hen, Differential control of learning and anxiety along the dorsoventral axis of the dentate gyrus. *Neuron* **77**, 955–968 (2013). doi:10.1016/j.neuron.2012.12.038 Medline

66. R. M. J. Deacon, J. N. P. Rawlins, T-maze alternation in the rodent. *Nat*. *Protoc*. **1**, 7–12 (2006). doi:10.1038/nprot.2006.2 Medline